Impact of Installation Effects on Optimal Propeller Design: Application to a Boundary-Layer-Ingesting Propeller

Barara, D.; van Sluis, M.; Sinnige, T.

DOI
10.2514/6.2024-3522

Publication date
2024

Document Version
Final published version

Published in
AIAA Aviation Forum and ASCEND co-located Conference Proceedings

AIAA Aviation Forum and ASCEND co-located Conference Proceedings
29 July - 2 August 2024, Las Vegas, Nevada
AIAA AVIATION FORUM AND ASCEND 2024
10.2514/6.2024-3522

Impact of Installation Effects on Optimal Propeller Design: Application to a Boundary-Layer-Ingesting Propeller

Daamanjyot Barara*, Martijn van Sluis†, and Tomas Sinnige‡
Delft University of Technology, 2629 HS Delft, The Netherlands

Propellers have gained traction in recent years and are subsequently being integrated into unconventional airframe configurations as part of conceptual designs for developing sustainable aircraft. Close coupling of the propeller and airframe enhances the non-uniformity of the inflow to the propeller. This non-uniform inflow introduces unsteady loading, affecting the propeller's performance. This paper investigates the impact of accounting for installation effects during propeller blade design within an optimization toolchain. This toolchain is applied to a propeller mounted at the rear of a fuselage utilizing Boundary Layer Ingestion (BLI). The proposed design methodology utilizes existing analysis methods to assess the installed aerodynamic and structural performance of the propeller. A gradient-based optimizer is coupled to these analysis methods to design two distinct blades for a multi-segment mission with the objective to maximize the aerodynamic performance. The geometry of the first propeller blade is optimized for the uniform inflow and consequently optimized to operate in the non-uniform inflow. The second blade is from the outset designed for the non-uniform inflow condition. The implementation of the proposed design methodology captures the sensitivity of the inflow field within the design loop, resulting in two distinct blade designs. Upon comparing these blades in BLI inflow conditions to meet identical performance requirements, it was observed that the blade designed to account for installation effects featured a higher inboard chord distribution and consumed 1.58% less energy compared to the blade optimized for uniform inflow for the considered mission profile.

Nomenclature

c	=	Chord, m
D	=	Propeller diameter, m
E	=	Energy consumption, J
f	=	Objective function
g	=	Equality constraint
h	=	Inequality constraint
J	=	Advance ratio; $V/(nD)$
n	=	Rotational speed, 1/s
P	=	Shaft power, W
P_C	=	Power coefficient; $P/(\rho V^3 D^2)$
T	=	Thrust, N
T_C	=	Thrust coefficient; $T/(\rho V^2 D^2)$
t	=	Time, mins; and Sectional thickness, m
u, v, w	=	Velocity in Cartesian system, m/s
V	=	Velocity, m/s
x, y, z	=	Cartesian coordinates, m
z	=	Sectional camber, m
β	=	Blade pitch angle, deg
ρ	=	Freestream air density, kg/m^3

*Researcher, Flight Performance and Propulsion, Delft University of Technology.
†PhD Candidate, Flight Performance and Propulsion, Delft University of Technology.
‡Assistant Professor, Flight Performance and Propulsion, Delft University of Technology.

σ = Normal stress, MPa
σ_y = Yield tensile strength, MPa
θ = Twist angle, deg

I. Introduction

Given its good aerodynamic efficiency at moderate subsonic Mach number, propellers have garnered significant interest amongst the research community as a step towards developing sustainable aircraft designs for short-range air travel. Several studies have proposed airframe configurations that leverage the aerodynamic performance of the propeller by strategically installing it in close proximity to the airframe to benefit in terms of aero-propulsive efficiency. Wingtip-mounted propellers [1], over-the-wing [2] and boundary-layer-ingestion (BLI) propellers [3, 4] are some examples of such configurations employing propellers to enhance the aerodynamic performance of the aircraft at the system level.

Installing a propeller in such an integrated configuration has a strong coupling with the airframe. Unlike an isolated propeller operating in undisturbed freestream, a propeller operating in such an integrated configuration ingests a flow with spatially varying velocity distribution at the propeller plane. Such a variation can impact the propeller's performance, potentially causing issues such as separation along the hub. Therefore, to reap the benefits of the configuration at the system level, it is crucial to understand whether the propeller blade design needs to be adapted to its local inflow field. The relative magnitude of the interaction between the propeller and the aircraft parts depends on the propeller's installation location [5].

To the author's knowledge, limited studies have been performed on propeller optimization in installed conditions compared to traditional propeller design research. Costa et al. [3] introduced a design methodology for propeller installed in BLI configuration. In their approach, the blade planform is modified for its aerodynamic performance through an optimization routine coupled with high-fidelity CFD to account for the interaction effects. Similarly, Pagano et al. [6] included high-fidelity fluid dynamics and structural dynamics computations in their optimization design routine to perform aeroacoustic optimization of a propeller blade installed in the pusher configuration downstream of a wing. Both studies showed that the inclusion of non-uniform effects can significantly affect the optimal blade design and propeller performance. However, using high-fidelity computations in the preliminary design study can be prohibitive due to the high computational power and time required. Sinnige et al. [7] presented a rapid blade design toolchain for aeroacoustic optimization of propellers in installed conditions. For the case of BLI inflow, the inclusion of installation effects within the optimization toolchain for aerodynamic performance resulted in a blade geometry with increased solidity and lower energy consumption compared to the design optimized for uniform inflow. However, this study did not include structural modeling in the design toolchain.

This work presents a rapid propeller blade optimization toolchain aimed at designing aerodynamically optimal propeller blades operating in a non-uniform inflow while adhering to the structural constraints to obtain realistic blade shapes. This toolchain is used to investigate the impact of including installation effects on both the optimal blade design and performance of the propeller, which could be a relevant consideration during the preliminary design phase of a propeller.

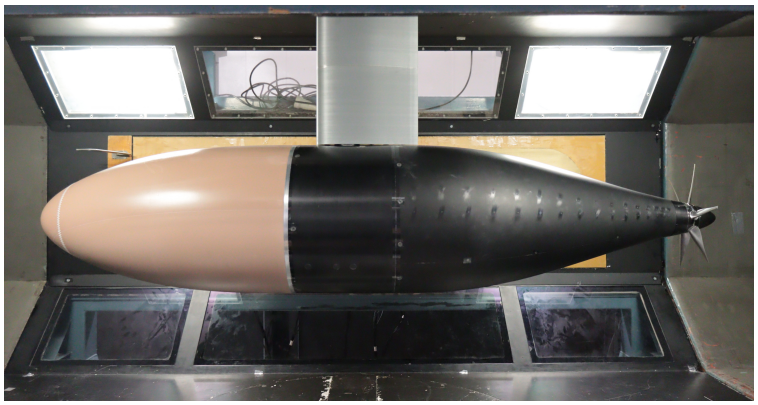

Fig. 1 Model in the test section of TU Delft's Low Turbulence Tunnel for which the propeller blades are being designed in this study. The direction of the flow is from left to right.

The proposed methodology is applied to design a propeller blade operating within the inflow of a fuselage boundary layer. The blades are intended to be designed for future experimental wind tunnel tests involving a model featuring a fuselage with a propeller in BLI configuration. Figure 1 shows the model of the fuselage used for the design studies. The geometry of the fuselage represents that of a conventional passenger aircraft and is designed according to the Engineering Science Data Unit (ESDU) guidelines. The designed propellers will be installed on the aft section of the fuselage.

The remainder of the paper is organized as follows: Section II briefly describes the aerodynamic and structural analysis tools implemented in this design study. Section III presents the optimization framework, detailing the definition of the objective function, design variables, and parameterization. This section also highlights the approach adopted for performing optimization studies to obtain blade designs optimized for non-uniform inflow conditions. The definition of the mission profile and performance requirements are presented in Section IV. The proposed design methodology is used to perform optimization studies and investigate the influence of including installation effects within the propeller design loop, the results of which are presented and discussed in Section V. Finally, Section VI presents the conclusions drawn from the results of this study.

II. Analysis Tools

The optimization routine utilizes aerodynamic and structural tools to compute the performance parameters, driving the optimizer towards an optimal blade design to minimize the cost function while adhering to structural constraints. The choice of analysis methods to be incorporated into the optimization routine is based on the following considerations –

- The method should be computationally efficient enough to be incorporated into optimization.
- The method should be sufficiently accurate in capturing the main sensitivities in aerodynamic performance as a response to changes in the inflow.

The following section presents a brief discussion of the aerodynamic and structural models implemented in the current design process for the performance prediction of the propeller, both in isolated and installed conditions.

A. Aerodynamics Model

The aerodynamic analysis model used in the current research is similar to the ones used by Sinnige et al. [7].

1. Aerodynamics Model for Isolated Propeller

The aerodynamic performance of the isolated propeller was computed using blade-element-momentum theory (BEMT). The application of this model provides the radial distributions of the loads along the blade for given freestream conditions and the propeller's operational settings. These loads are further used to compute the thrust generated and power required by the propeller in the isolated condition. Since these aerodynamic loads serve as input for predicting both the installed performance of the propeller and the structural model, it is crucial for the model's predictions to be sufficiently accurate. As noted by Gur and Rosen [8], the BEMT strikes a favorable balance between accuracy and computational cost compared to other aerodynamic prediction models for propellers. This makes it an attractive choice for inclusion in the current optimization study. Consequently, the BEMT model is used to compute the aerodynamic performance of the propeller.

BEMT discretizes the propeller blade into radial sections, considering each section as an airfoil. It utilizes the aerodynamic characteristics of 2-dimensional airfoils to predict blade loadings and overall propeller performance. The aerodynamic database of the airfoils is constructed by determining their aerodynamic characteristics across a wide range of angles of attack and Reynolds numbers using XFOIL [9]. The post-stall airfoil method developed by Viterna [10] is employed to predict the lift and drag coefficients of the airfoils beyond the stall angle and extend the range of airfoil polars. Furthermore, the Prandtl-Glauert correction is applied to consider compressibility effects on the blade sections, while Prandtl's tip loss factor is used to account for root and tip losses.

2. Aerodynamics Model for Installed Propeller

In order to assess the propeller's aerodynamic performance in installed condition, the aerodynamic analysis tool is based on an engineering method coupling BEMT and non-uniform inflow field at the propeller plane. A detailed explanation of this engineering method can be found in Ref.[4]. This approach for computing blade load distribution due to non-uniform inflow relies on two inputs - a) Non-uniform inflow field at the propeller plane using CFD, and b) Propeller's performance in uniform condition.

This approach is based on the assumption that, in the installed condition, non-uniformity of the inflow field would induce a local disturbance in the propeller's blade loading at its nominal operating condition, i.e., its performance in undisturbed uniform inflow. The disturbance due to this induction would lead to a change in the local advance ratio $\Delta J'$ at a given radial position, which in turn causes variations in the thrust and torque loads. By imposing the inflow field onto the propeller disk, the local change in advance ratio, $\Delta J'$, is determined at radial locations for different azimuthal positions. Once the change in local advance ratio is determined, the loading distribution at different azimuthal positions around the propeller disk is computed by interpolating over the performance maps of the isolated propeller that was obtained using BEMT. After determining the load distribution for each azimuthal position, the integral propeller forces are computed by integrating over the propeller disk.

In this method, the non-uniform inflow should be known a priori and is determined using CFD, accounting for the interference effects that a propeller would encounter at the position of its operation due to the presence of the airframe. The coupling between the propeller and inflow is neglected in this approach. Additionally, to evaluate the performance of the installed propeller, performance maps of isolated propeller have to be generated for a range of advance ratios. In the current implementation of the method, BEMT has been coupled directly into the aerodynamic solver. During the optimization process, BEMT will be used for each function evaluation to compute performance maps for each blade design and setting. This method computes the blade loading distribution in a quasi-steady manner, upon which the unsteady effects are accounted for by applying the Sears function to the blade forces.

B. Structural Model

1. Aerostructural Model for Isolated Propeller

The structural model is crucial for imposing structural constraints within the optimization routine such as limits on the allowable stress and maximum twist deflection. In the current tool, this aerostructural model is based on the approach proposed by Sodja et al. [11]. This approach uses Euler–Bernoulli beam theory and Saint–Venant theory of torsion to account for bending and torsional deformations of the blades, respectively. This method treats the propeller blades as slender, pre-twisted cantilever beams of variable cross-sections built out of homogenous and isotropic material.

The aerostructural solver combines aerodynamic loads from the aerodynamic solver with inertial loads to compute moments along the local coordinate axis of the blade at various radial positions. Once the moments due to the aerodynamic and inertial loads are calculated, the blade's deformation and stresses are determined. In the current model, blade deformation is contributed by - bending and torsion. Assuming that the blade cross section is solid, the warping effects are neglected as they would be minimal.

2. Aerostructural Model for Installed Propeller

A quasi-steady approach has been used to extend Sodja et al.'s model [11] for predicting the structural loads experienced by the blade during rotation around the disk in non-uniform inflow conditions. By determining the radial aerodynamic load distributions at each azimuthal position around the propeller disk, the structural solver computes moments and deflections at each of these positions. This results in the computation of the moments, stresses, in-plane and out-of-plane deflections over the propeller disk due to the non-uniformity in the inflow field. These are further used as a condition to be satisfied by the optimizer to obtain an optimal blade design that is structurally realizable. It must be noted that the vibrations induced due to the unsteady effects of non-uniform inflow are neglected for the prediction of structural loads of an installed propeller.

III. Optimization Framework

Optimizations are performed to assess the influence of installation effects on the optimal blade design, optimized for aerodynamic performance while meeting performance and structural constraints, across a multi-segment mission profile. A gradient-based method is used in combination with propeller analysis methods within the current framework to design two blades: a) a blade optimized for isolated conditions, and b) a blade optimized for the installed condition. Figure 2 depicts the workflow of the optimization framework along with its components. The same framework has been utilized to optimize both blades, with the only difference being the replacement of the aerodynamic and aerostructural models specific to each case.

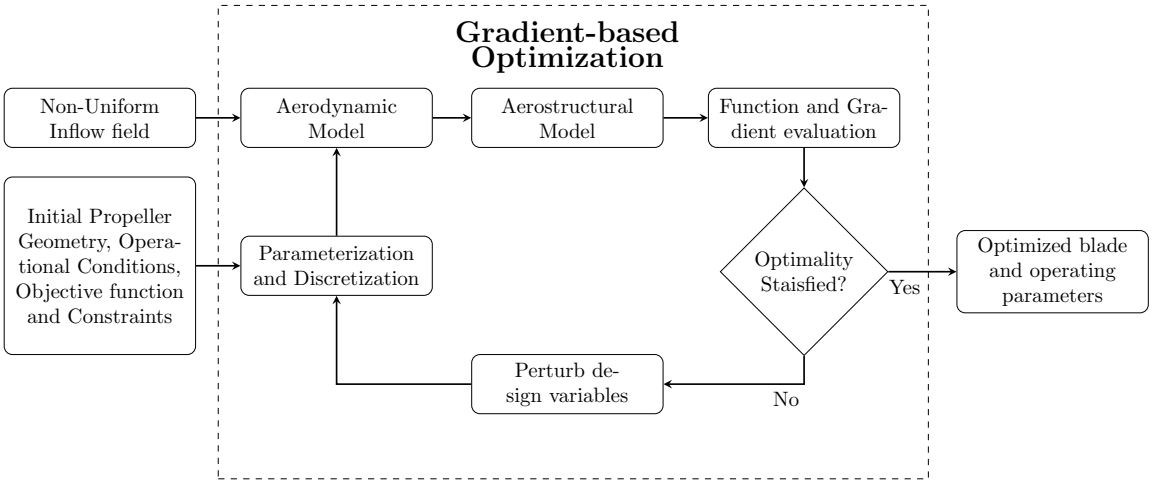

Fig. 2 Workflow of the optimization framework and its components.

A. Definition of Objective Function and Constraints

In the current study, optimizations have been performed to achieve optimal aerodynamic performance of the propeller blade, which translates to minimizing energy consumption over the entire mission. The energy consumption of the propeller blade is derived from its shaft power P, and the total energy consumption E over each of the mission segments can be defined as,

$$E = \sum_{i=1}^{N} E_i = \sum_{i=1}^{N} P_i t_i \tag{1}$$

where, i indicates the mission segment, N refers to the number of mission segments, and t is the time duration of each of the mission segments. To avoid scaling issues during the design search, the objective function f is defined by normalizing the energy consumption with that of the initial design,

$$f = \frac{E}{E_0} \tag{2}$$

where, E_0 represents the energy consumption of initial design. Throughout the rest of this paper, subscript '0' will be used to denote the quantities of the initial design.

The optimization process is constrained by performance and structural requirements that the optimal blade design must satisfy, and this is expressed through equality and inequality constraints within the optimization loop. To ensure that the optimal blade design meets the thrust requirement for each of the mission segments, the equality constraint is defined as,

$$g_i = \frac{T_i}{T_{i\text{req}}} - 1 = 0 \tag{3}$$

where, $T_{i\text{req}}$ is the thrust requirement from the blade for each mission segment i.

To prevent the blades from being too slender and experiencing high twist deflections, which could compromise both the structural integrity and aerodynamic performance of the blades, inequality constraints were defined as,

$$h_i = \begin{bmatrix} \frac{F.S.*\sigma_i}{\sigma_y} - 1 \\ \frac{\Delta\beta_i}{\Delta\beta_{\max}} - 1 \end{bmatrix} \leq 0 \tag{4}$$

where, σ_y is the yield stress of the material and *F.S.* is the structural factor of safety that is applied to the maximum von Mises stress σ_i experienced by the blade during its operation in the mission segment i. $\Delta\beta_i$ is the twist deflection along the blade in the mission segment i and is limited by the maximum twist deflection $\Delta\beta_{\max}$. The values of performance and structural requirements specific to the test case under consideration are defined in Section IV.

B. Design Variables and Geometry Parameterization

The definition of design parameters that dictate the propeller's geometrical design plays a crucial role in the optimization process. The propeller's geometrical design and operational condition are used as variables in the current study and can be categorized into the following -

- Operational Parameters - Rotational speed n and collective pitch setting at 70% radial position $\beta_{0.7Rp}$, for each of the mission segments.
- Blade Planform Parameters - Radial chord distribution $c(r)$, radial twist distribution $\theta(r)$, and propeller diameter D.
- Sectional Parameters - Radial thickness/chord distribution $t/c(r)$ and radial camber distribution $z/c(r)$.

1. Airfoils and Sectional Parameters

The sectional parameters have been defined using the airfoil parameters, namely the thickness/chord ratio and camber, which can influence the aerodynamic and structural performance of the propeller. Therefore, these sectional variables are crucial for achieving optimal blade design, allowing for the exploration of a wide design space. Given its exceptional performance for a wide range of flow conditions, the family of ARA-D airfoils has been chosen for the propeller design [12]. The 6-bladed TUD-XPROP, one of TU Delft's reference propellers, uses airfoils derived from the ARA-D family of airfoils. To generate a wide dataset of airfoils for use in the current study, the airfoil profiles at different radial sections of TUD-XPROP were extracted and modified. Each of these airfoils can be defined based on - thickness/chord ratio, camber, and chordwise position of maximum camber. Due to the marginal difference in the chordwise position of maximum camber among the baseline airfoils, this parameter was omitted from modification. The baseline airfoils were modified such that, for a given thickness/chord ratio, a range of profiles was generated by varying the maximum camber as a percentage of the chord using XFOIL's 'Geometry Design Routine (GDES)' [9]. The maximum camber percentage for each thickness/chord ratio ranges from 1% to 5%. In this way, a new set of airfoils is generated by modifying baseline ARA-D profiles solely based on two parameters: thickness/chord ratio and camber. The final airfoil dataset includes sections with thickness/chord ratios ranging from 5% to 23% and camber ranging from 1% to 5%.

2. Geometry Parameterization

To mathematically define the planform of the propeller blade while guaranteeing smooth distribution, cubic Bezier curve parameterization is used to describe the chord, twist, thickness, and camber distribution along the span.

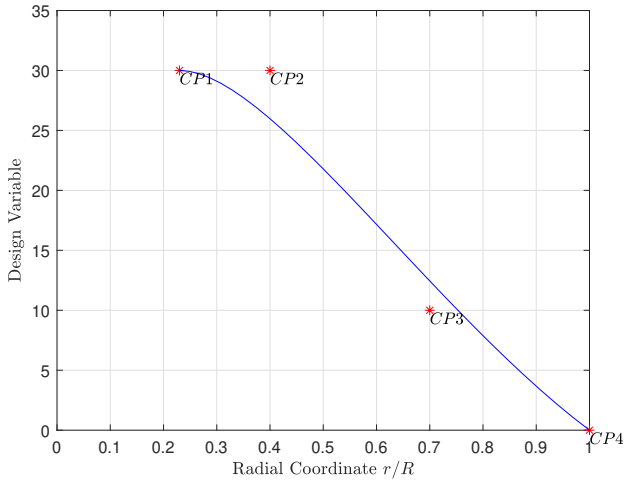

Fig. 3 Representation of a cubic Bezier curve.

To describe the radial distribution of the blade's planform and sectional parameters, the position of control points is defined by two dimensions: parameter value and radial position. The radial positions of the first and last control points, at the root and tip respectively, are fixed, while the intermediate control points have the freedom to move within the

design space in two dimensions. Alongside fixing the first and last control points in the radial direction, the last control point for twist distribution, which represents the twist at the blade tip, is fixed to 0. Therefore, only 5 design variables are required to define the blade's twist distribution, while 6 design variables are needed to define the radial distribution of chord, thickness/chord ratio, and camber along the blade. The bounds on these parameters for the current case will be defined in Section IV.

C. Design Approach

In this design study, optimizations have been performed for propellers operating in different inflow conditions. For clarity, Table 1 presents an overview of the configurations of interest that have been used in this paper.

Table 1 Overview of propeller geometries and conditions in which they are assessed in this design study.

Parameter	Description
iso-iso	Propeller optimized for isolated condition and operating in isolated condition.
iso-ins	Propeller optimized for isolated condition and operating in installed condition.
ins-ins	Propeller optimized for installed condition and operating in installed condition.

1. Isolated Propeller Design

In the case of isolated propeller optimization, a two-step approach has been adopted which dictates the definition of the objective function and constraints. As a first step for the isolated propeller design, the blade is optimized for the undisturbed uniform flow condition. The optimization problem for this step can be formulated as,

$$\begin{aligned} &\textit{minimize} && \frac{E_{\text{iso-iso}}}{E_{\text{iso-iso}0}} = f(n_i, \beta_{0.7R_{P\,i}}, c(r), \theta(r), t/c(r), z/c(r), D) \\ &\textit{subject to} && T_i = T_{i\text{req}} \\ & && F.S. * \sigma_i \leq \sigma_y \\ & && \Delta\beta_i \leq \Delta\beta_{\max} \end{aligned}$$

To study the impact of the installation effects on the blade design optimization and to draw a fair comparison with the installed design, the isolated blade design must meet the performance requirements under installed conditions. Since the performance of the isolated blade would vary in the installed condition, a second optimization step was required to determine the optimal operational parameters of the isolated blade design in the flowfield associated with the installed condition. The blade design remains unchanged for this step. The optimization problem for this step can be formulated as,

$$\begin{aligned} &\textit{minimize} && \frac{E_{\text{iso-ins}}}{E_{\text{iso-ins}0}} = f(n_i, \beta_{0.7R_{P\,i}}) \\ &\textit{subject to} && T_i = T_{i\text{req}} \\ & && F.S. * \sigma_i \leq \sigma_y \\ & && \Delta\beta_i \leq \Delta\beta_{\max} \end{aligned}$$

2. Installed Propeller Design

In the case of installed propeller design, the effects of non-uniform inflow have been included within the optimization loop. To initiate this optimization, optimal geometric parameters derived from the blade design of the isolated propeller and its optimal operational parameters in the non-uniform inflow were used as the starting point. The optimization problem for installed propeller design can be formulated as,

$$\textit{minimize} \quad \frac{E_{\text{ins-ins}}}{E_{\text{ins-ins}0}} = f(n_i, \beta_{0.7R_{P\,i}}, c(r), \theta(r), t/c(r), z/c(r), D)$$

$$\textit{subject to} \quad T_i = T_{i\,\text{req}}$$
$$F.S. * \sigma_i \leq \sigma_y$$
$$\Delta\beta_i \leq \Delta\beta_{\max}$$

D. Optimization Algorithm and Tolerances

The gradient-based optimizations are performed using sequential quadratic programming (SQP) algorithm. The gradients are estimated using the forward finite differences method during optimization. Tolerances imposed on the first-order optimality, maximum constraint violation, and minimum change in the design variables are 10^{-4}, 10^{-5}, and 10^{-5}, respectively.

IV. Problem Definition

The proposed methodology has been applied to derive optimal blade designs for propellers operating in the boundary layer of a fuselage. The resulting blades will be manufactured and used in experimental tests as part of ongoing research. Therefore, the inflow fields, operating conditions, and performance criteria considered in this study are devised in accordance with future experimental tests.

The simplified mission profile comprises three segments: take-off, climb, and cruise. The operational conditions and performance requirements for these mission segments are listed in Table 2. Thrust requirements for the three mission segments are defined such that the resulting thrust coefficients are representative of those of a turboprop passenger aircraft. The values of thrust presented in Table 2 have been calculated to match the corresponding thrust coefficients under wind tunnel conditions during the upcoming experiments.

Table 2 Operating conditions and performance requirements for optimization.

Parameter	Take Off	Climb	Cruise
Freestream Velocity [m/s]	30	60	60
Time Duration [min]	2	10	40
Thrust requirement [N]	35.56	56.9	14.22

Table 3 lists the structural properties and requirements used in the optimization. It was decided to fix the number of blades of the propeller to 6 blades due to the availability of a suitable hub for the experimental campaign. The sensitivity of the results to the blade count has not been assessed in this study.

Table 3 Structural properties and constraints for optimization.

Parameter	Value
Material	Stainless Steel
Max yield tensile strength, σ_y	207 MPa
Structural factor of safety, $F.S.$	2.0
Max. twist deformation, $\Delta\beta_{\max}$	0.1°

The inflow field of the boundary layer ingestion at the propeller plane was obtained from a time-averaged uRANS solution modeling the wind tunnel setup. Figure 4 shows the inflow fields of the axial, lateral, and vertical velocity components at the propeller plane used in this study. From the inflow field contours at the propeller disk, it can be inferred that the propeller ingesting the boundary layer would operate in a spatially varying region of the velocity field in the axial, lateral, and vertical directions. The fuselage contraction, upsweep, boundary layer, and wake from the upstream fairing contribute to the non-uniformity in the velocity fields. The interaction of such non-uniformity with the

propeller blade gives rise to dynamic stresses. The presence of such dynamic loads emphasizes the need to account for the structural performance of the blades in the preliminary design phase.

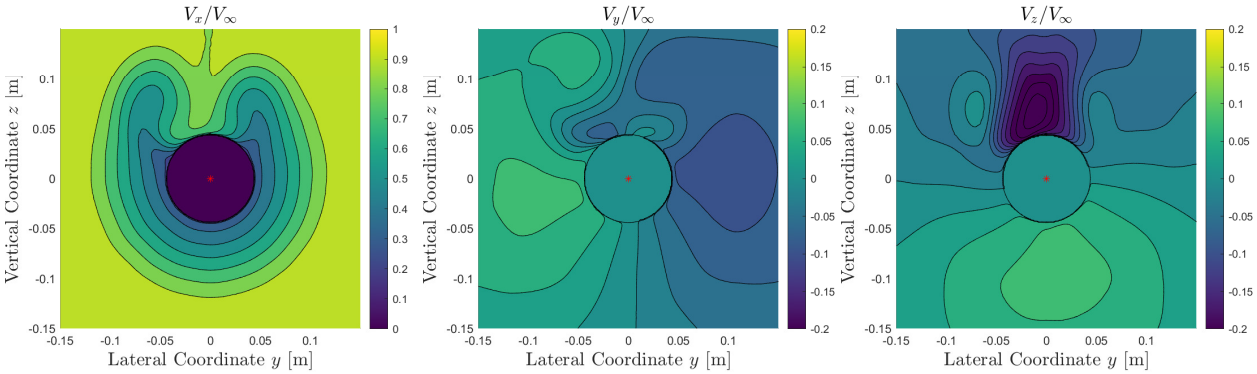

(a) Axial Velocity Component **(b) Lateral Velocity Component** **(c) Vertical Velocity Component**

Fig. 4 Inflow fields of Boundary Layer Ingestion considered in this study.

Based on the problem definition, 30 design variables were used in the optimization. Table 4 presents the design variables and the bounds imposed on them. In the first step of the isolated propeller design optimization, which was performed for uniform flow, 30 design variables were used. While, in the second step, 6 design variables defining the propeller's operational parameters were used to meet performance requirements in non-uniform inflow. The installed propeller design optimization was performed with 30 design variables for non-uniform inflow.

Table 4 Bounds on the design variables.

Design Variable	Lower Bound	Upper Bound	Parameter	Lower Bound	Upper Bound
n_{TO} [1/s]	40	157.48	$(r/R)^{\theta(r)}_{CP2}$	0.44	0.80
n_{CL} [1/s]	40	157.48	$(r/R)^{\theta(r)}_{CP3}$	0.55	0.95
n_{CR} [1/s]	40	157.48	$(t/c)^{t/c(r)}_{CP1}$	0.05	0.23
$\beta_{0.7R_pTO}$ [°]	0	60	$(t/c)^{t/c(r)}_{CP2}$	0.05	0.23
$\beta_{0.7R_pCL}$ [°]	0	60	$(t/c)^{t/c(r)}_{CP3}$	0.05	0.23
$\beta_{0.7R_pCR}$ [°]	0	60	$(t/c)^{t/c(r)}_{CP4}$	0.05	0.23
$c^{c(r)}_{CP1}$ [m]	0.006	0.035	$(r/R)^{t/c(r)}_{CP2}$	0.44	0.80
$c^{c(r)}_{CP2}$ [m]	0.006	0.035	$(r/R)^{t/c(r)}_{CP3}$	0.55	0.95
$c^{c(r)}_{CP3}$ [m]	0.006	0.035	$(z/c)^{z/c(r)}_{CP1}$	0.01	0.05
$c^{c(r)}_{CP4}$ [m]	0.006	0.035	$(z/c)^{z/c(r)}_{CP2}$	0.01	0.05
$(r/R)^{c(r)}_{CP2}$	0.44	0.80	$(z/c)^{z/c(r)}_{CP3}$	0.01	0.05
$(r/R)^{c(r)}_{CP3}$	0.55	0.95	$(z/c)^{z/c(r)}_{CP4}$	0.01	0.05
$\theta^{\theta(r)}_{CP1}$ [°]	10	40	$(r/R)^{z/c(r)}_{CP2}$	0.44	0.80
$\theta^{\theta(r)}_{CP2}$ [°]	0	30	$(r/R)^{z/c(r)}_{CP3}$	0.55	0.95
$\theta^{\theta(r)}_{CP3}$ [°]	-10	30	R [m]	0.102	0.152

Before initiating the optimization, the initial values of the design variables are scaled based on their bounds. This is done to avoid scaling issues, as gradient-based methods are susceptible to these, which can reduce the effectiveness of the optimization [13]. The optimizer uses the scaled version of the design variables, but for modeling purposes, the design variables are scaled back to their original values.

V. Results and Discussion

The proposed methodology is applied to the preceding problem definition, with the goal of designing blades that minimize total energy consumption throughout the entire proposed mission profile. The optimization results of the isolated propeller blade and installed propeller blade in the non-uniform inflow field are presented and discussed. The discussion of results highlights how incorporating the interaction effects of boundary layer ingestion within the optimization process of blade design impacts both the aerodynamic and structural performance of the propeller blade.

A. Overall Performance and Optimal Blade Designs

The optimized blade designs are shown in Fig. 5. As can be inferred from the figure, the two blades have distinct geometric features but a marginal difference in tip radius. The isolated blade design features a slightly larger tip radius of 152.2 mm, in contrast to the installed blade design with a tip radius of 151.8 mm. Based on volume, the installed blade has 89.5% more volume than the isolated blade.

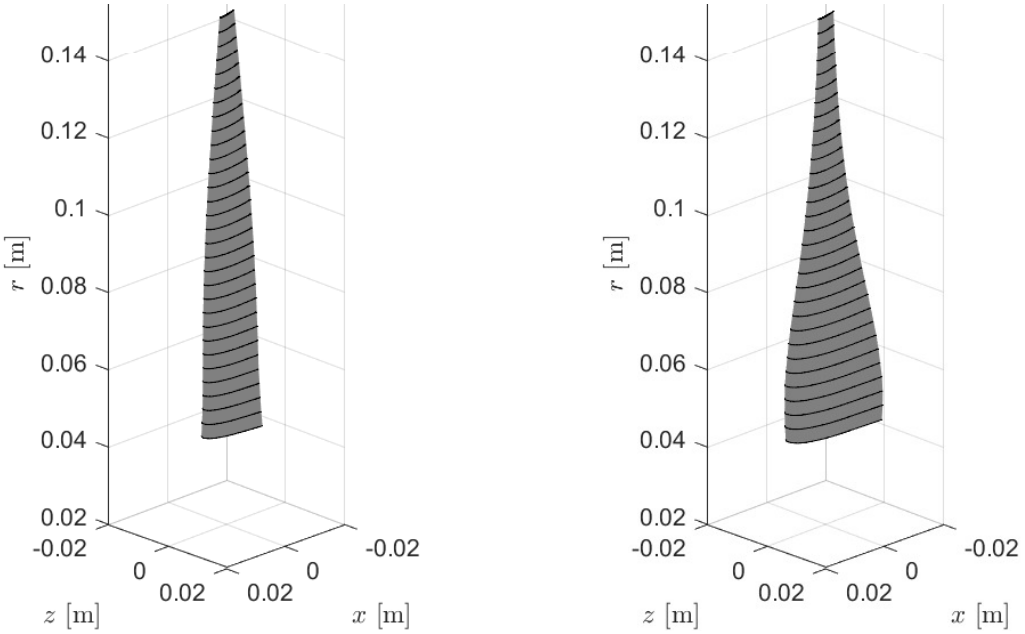

(a) Optimized isolated propeller blade. **(b) Optimized installed propeller blade.**

Fig. 5 Optimized propeller blades.

Table 5 and 6 present a comparison between performance and the optimal operational parameters of the two optimized blades for each mission segment when operating in the installed condition, respectively. Figure 6 shows the radial distributions of the geometrical characteristics of the optimized blades.

Table 5 Impact of boundary layer ingestion inflow on the performance of the optimized blades.

Performance Parameter		Isolated Opt.	Installed Opt.	(Ins.-Iso.)/Iso.
Energy Consumption [MJ]	E_{TO}	0.152	0.151	-0.18%
	E_{CL}	2.10	2.05	-2.18%
	E_{CR}	1.75	1.73	-0.98%
	E_{total}	4.01	3.94	-1.58%
Figure of Merit [-]	T_C/P_{CTO}	0.841	0.843	+0.19%
	T_C/P_{CCL}	0.974	0.996	+2.23%
	T_C/P_{CCR}	1.16	1.18	+0.99%

Table 6 Impact of boundary layer ingestion inflow on the operational design parameters of the optimized blades.

Operational Parameter		Isolated Opt.	Installed Opt.	(Ins.-Iso.)/Iso.
Rotational Speed [1/s]	n_{TO}	146.54	137.23	-6.35%
	n_{CL}	157.48	157.48	+0.0%
	n_{CR}	110.95	114.97	+3.62%
Collective pitch [°]	$\beta_{0.7R_pTO}$	23.8	25.9	+8.82%
	$\beta_{0.7R_pCL}$	37.2	36.2	-2.71%
	$\beta_{0.7R_pCR}$	36.3	34.4	-5.21%

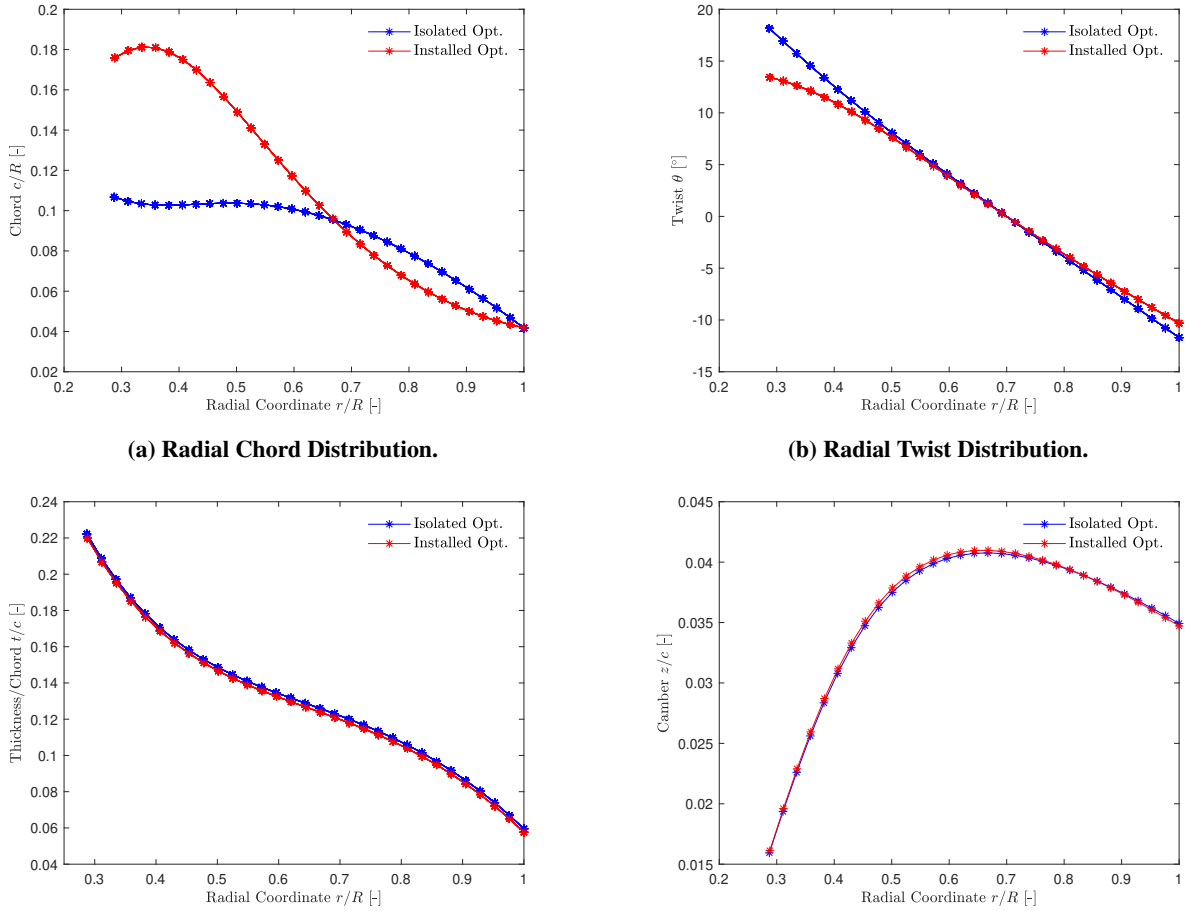

(a) Radial Chord Distribution.

(b) Radial Twist Distribution.

(c) Radial Thickness Distribution.

(d) Radial Camber Distribution.

Fig. 6 Geometry of optimized blades.

It can be noted from Table 5 that the installed design consumes 1.58% less overall energy over the full mission profile as compared to the isolated design. The largest difference in energy consumption between the two blades is observed during the climb phase, where the installed design operates with 2.18% lower energy than the isolated design to produce identical thrust. In contrast, the take-off phase shows the least difference, with the installed design consuming 0.18% less energy compared to the isolated design. Table 5 also compares the two blades based on a figure of merit, T_C/P_C, which is the ratio of the propeller's thrust coefficient to its power coefficient, defined based on freestream conditions. This figure of merit serves as a performance metric and is equivalent to the definition of propeller efficiency for an isolated propeller operating in undisturbed uniform flow. Similar to the trends in energy consumption, the installed

design exhibits relatively better performance with higher T_C/P_C values in all mission phases compared to the isolated design. The largest gain of 2.23% in T_C/P_C is observed in the climb phase.

From Table 6, it can be inferred that the installed design tends to operate at a lower pitch angle compared to the isolated design, with differences of -2.71% in the climb phase and -5.21% in the cruise phase. This reduction in collective pitch is accompanied by an increase in rotational speed for the installed design during cruise, with its rotational speed being 3.62% higher than that of the isolated design. However, there is no difference in the rotational speeds of the two designs during the climb phase, as both blades operate at the upper bound set on the rotational speed in the optimization. Among all mission segments, the climb phase has the highest thrust requirement, potentially leading the optimizer toward the upper bound of rotational speed. In contrast to the climb and cruise phase, the installed design operates at 8.82% higher pitch angle and 6.35% lower rotational speed during the take-off phase when compared to the isolated design.

As can be inferred from Fig. 6a, the inclusion of boundary layer ingestion inflow within the optimization loop leads to a wider chord distribution along the inboard part of the installed design compared to the isolated design. Whereas, the outboard portion of the installed blade exhibits a relatively slender chord distribution. Because the inboard section of the blade encounters low axial velocity due to boundary layer ingestion inflow, the optimizer takes advantage of the 'BLI' benefit. This involves improving the performance by adding higher energy into the slower-moving flow. Therefore, in this region of reduced flow, higher loading is attained in the inboard portion by having a longer chord. Such a trend in the blade designs is also observed in the works of Sinnige et al. [7] and Lv and Rao [14] focusing on boundary layer ingestion blade designs. Consequently, from Fig. 6b it can be inferred that the two blades have a varying radial twist distribution as the installed design has a lower twist angle in the inboard portion, which can be attributed to the reduction in the effective angles of attack in this portion. Figures 6c and 6d show marginal differences in the distribution of thickness/chord ratio and camber along the blade span between the two designs.

B. Aerodynamic Performance in Installed Condition

Figure 7 shows the contours and plots of loading distributions of the two optimized propeller blades in terms of thrust coefficient T_C when operating at the design point during the climb phase. Since the climb segment had the highest thrust requirement, it represented the limiting case in the current study. Therefore, the performance of the propellers during the climb phase is shown here. The radial distribution of the thrust coefficient is depicted along the azimuthal position where the largest value of T_C occurs on the propeller disk, as shown in the contours of Fig.7. Figure 7 suggests that the installed blade has higher loading towards the inboard portion compared to the isolated design. This difference in loading distribution can be attributed to the increased chord distribution on the inboard section of the installed design.

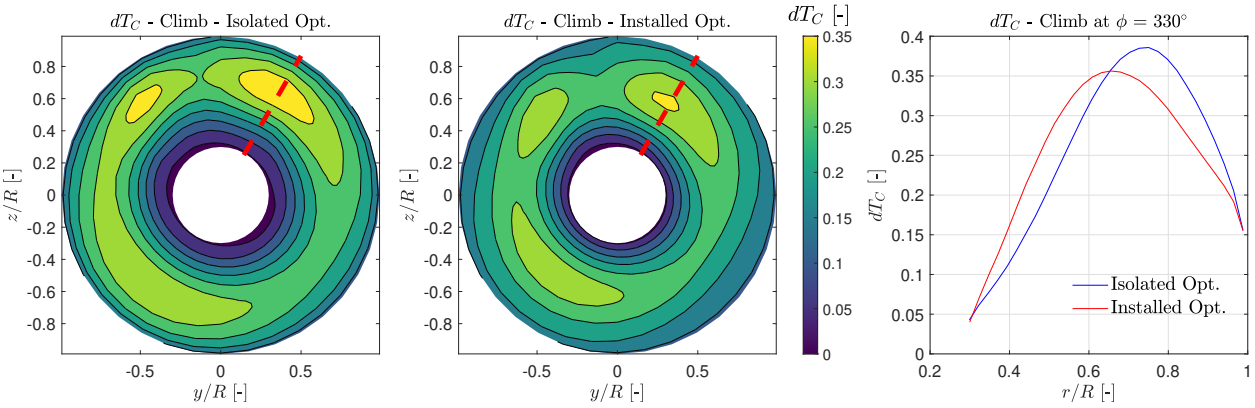

Fig. 7 Impact of the installation effects on the distribution of thrust coefficient of the optimized blades during the climb phase.

The distributions of T_C/P_C at the propeller disk for the climb segment of the two optimized propeller blades are shown in Fig.8. The survey line traces across the azimuthal position, passing through the region of high T_C/P_C values on the propeller disk. From the contours of two blades in Fig.8, it can be inferred that the magnitude of T_C/P_C is higher in the inboard section of the propeller disk and reduces towards the tip. On comparing the radial distributions of T_C/P_C for the two blades, the installed blade shows lower sectional values in the inboard section compared to the isolated

design. However, the sectional values of T_C/P_C are higher for the installed design towards the outboard section. Such a difference between the distribution of T_C/P_C can mainly be attributed to the differences in the solidity of the two blades, wherein a higher inboard chord distribution of the installed blade translates to a lower T_C/P_C value and vice versa. The variation in the chord distribution, and hence solidity, impacts the sectional efficiency [15]. Note that this conclusion is drawn by using T_C/P_C as a performance metric, which is equivalent to the propeller efficiency of an isolated propeller in uniform flow.

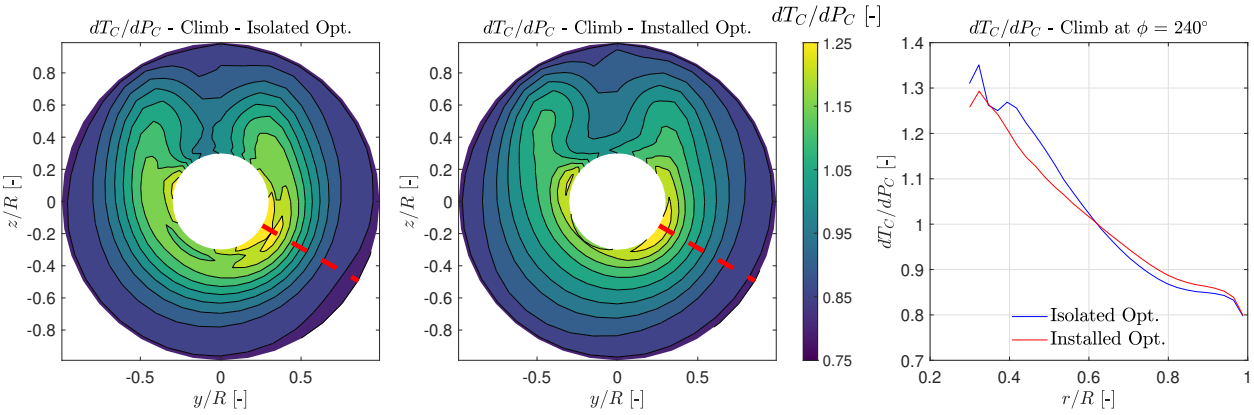

Fig. 8 Impact of the installation effects on the distribution of figure of merit, dT_C/dP_C, of the optimized blades during the climb phase.

C. Structural Performance in Installed Condition

Figure 9 shows the structural performance of the two optimized propeller blades in terms of radial distribution of stress normalized by the yield strength of the material, when operating at the design point during the climb phase. The survey line highlights the azimuthal position passing through the region of highest stress experienced by the two propeller blades. From Figure 9, it can be inferred that the two propeller blades differ significantly in terms of structural performance, as the isolated design experiences higher stresses in the inboard portion of the blade compared to the installed design. The variation in structural stresses can mainly be attributed to differences in chord and twist distribution between the two blades. The installed design exhibits increased solidity and decreased twist in the inboard section, resulting in lower inboard stresses. However, towards the outboard section ($r/R \sim 0.7$), where the chord distribution is lower, the installed design experiences relatively high stresses compared to the isolated design, as indicated by the radial distribution. Both blades conform to the structural stress constraint, as the maximum structural stress experienced by both remains below the normalized stress value of 0.5.

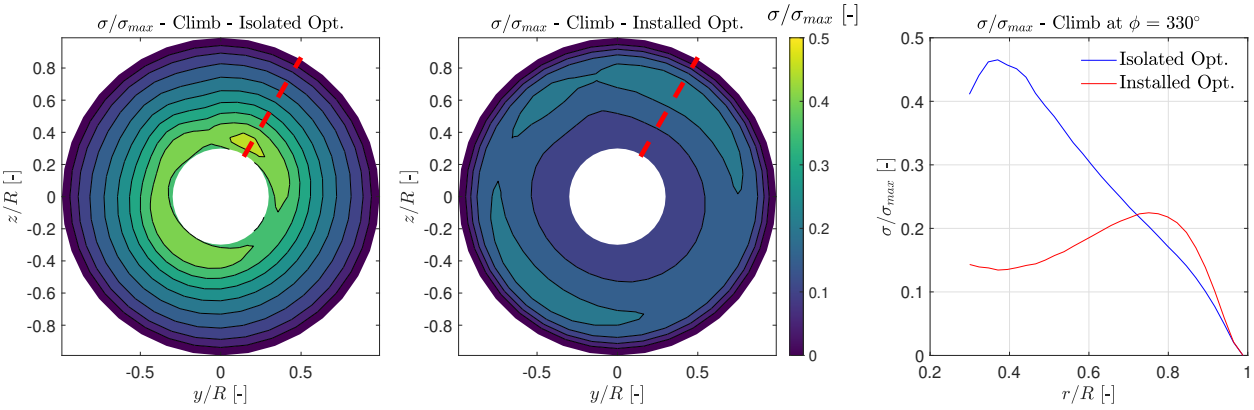

Fig. 9 Impact of the installation effects on the normalized stress distribution of the optimized blades in the climb phase.

The impact of installation effects on blade deflection during the climb phase is shown in Fig.10. The survey line is traced along the same azimuthal position where the highest stresses are encountered by both blades. It can be observed from the contours that the installed design exhibits lower deflection in blade angle in the inboard portion compared to the isolated design, attributed to its higher inboard solidity. The radial distribution shown in Fig. 10 further indicates that for the installed design, the deflection remains less than 0.02° up to the radial position $r/R \sim 0.7$. Both blades meet the constraint of maximum twist deflection of 0.1°. It is crucial to monitor this parameter for a propeller experiencing non-uniform inflow from the performance perspective, as significant deflection can alter the propeller's aerodynamic performance, deviating it from the intended performance.

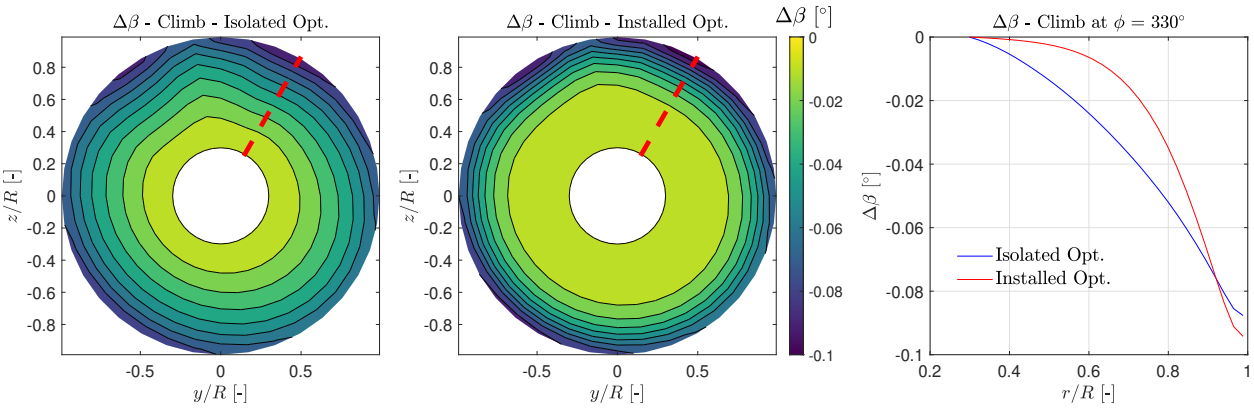

Fig. 10 Impact of the installation effects on the variation in blade angle of the optimized blades in the climb phase.

VI. Conclusions and Outlook

In this paper, we investigate the influence of incorporating installation effects within the design optimization loop using a rapid propeller design toolchain, while considering structural performance. Based on the results obtained regarding the inclusion of effects of boundary layer ingestion inflow during the optimal propeller blade design, the following conclusions can be drawn:

- The design methodology effectively captures the sensitivities of the inflow field within the design loop, resulting in two distinct blade designs. Incorporating the installation effects of BLI results in an installed design characterized by a higher inboard chord distribution and lower twist on the inboard section compared to the isolated design. This outcome is due to the optimizer leveraging the lower axial velocity in this region to enhance performance.
- Accounting for the installation effects of BLI inflow within the blade design optimization loop results in a 1.58% reduction in the total energy consumption for the installed blade compared to the isolated blade operating under the same inflow conditions. Maximum benefit in terms of lower energy consumption is achieved during the climb phase of the mission.
- The variation in geometry between the optimized blades, designed to meet identical performance requirements in BLI inflow conditions, leads to distinct aerodynamic and structural performances for a given mission segment. The installed design exhibits higher inboard loading, while its increased solidity significantly reduces stresses in the inboard portion compared to the isolated blade.

Following this study, future work plans on implementing the structural tools with improved fidelity, allowing for the capability to model the structural loads for non-isotropic materials. An aeroacoustic model will be integrated into the design toolchain to address the acoustic performance of the installed propellers. This approach could contribute to the preliminary design of optimal blades that are both low-noise and highly efficient, while also ensuring structural feasibility.

VII. Acknowledgements

The authors would like to thank Jatinder Goyal [16], Nando van Arnhem, and Manthan Sharma for providing the baseline codes for the development of the toolchain presented. This project has been financed by the Dutch Ministry of

Economic Affairs and Climate under the TKI scheme (Grant number TKI HTSM/18.0170) along with SAFRAN Tech.

References

[1] Miranda, L., and Brennan, J., "Aerodynamic Effects of Wingtip-Mounted Propellers and Turbines," *4th Applied Aerodynamics Conference*, 1986, p. 1802.

[2] Müller, L., Heinze, W., Kožulović, D., Hepperle, M., and Radespiel, R., "Aerodynamic Installation Effects of an Over-the-Wing Propeller on a High-Lift Configuration," *Journal of Aircraft*, Vol. 51, No. 1, 2014, pp. 249–258.

[3] Paula Costa, F., Tomita, J. T., Silva, V. T., Andersson, N., Grönstedt, T., and Bringhenti, C., "Aerodynamic Analysis of Conventional and Boundary Layer Ingesting Propellers," *Journal of Engineering for Gas Turbines and Power*, Vol. 145, No. 1, 2023, p. 011024.

[4] van Arnhem, N., de Vries, R., Sinnige, T., Vos, R., Eitelberg, G., and Veldhuis, L. L., "Engineering Method To Estimate the Blade Loading of Propellers in Nonuniform Flow," *AIAA Journal*, Vol. 58, No. 12, 2020, pp. 5332–5346.

[5] The Royal Aeronautical Society, "Introduction to Installation Effects on Thrust and Drag for Propeller-Driven Aircraft," Tech. Rep. ESDU 85015, August 2006.

[6] Pagano, A., Barbarino, M., Casalino, D., and Federico, L., "Tonal and Broadband Noise Calculations for Aeroacoustic Optimization of a Pusher Propeller," *Journal of Aircraft*, Vol. 47, No. 3, 2010, pp. 835–848.

[7] Sinnige, T., de Gruijl, W., de Haan, W., and Eitelberg, G., "Rapid Aeroacoustic Planform Design Optimization of Installed Propellers," *33rd Congress of the International Council of the Aeronautical Sciences*, 2022, pp. 2022–0489.

[8] Gur, O., and Rosen, A., "Multidisciplinary design optimization of a quiet propeller," *14th AIAA/CEAS Aeroacoustics Conference (29th AIAA Aeroacoustics Conference)*, 2008, p. 3073.

[9] Drela, M., "XFOIL: An analysis and design system for low Reynolds number airfoils," *Low Reynolds Number Aerodynamics: Proceedings of the Conference Notre Dame, Indiana, USA, 5–7 June 1989*, Springer, 1989, pp. 1–12.

[10] Viterna, L. A., and Janetzke, D. C., "Theoretical and experimental power from large horizontal-axis wind turbines," Tech. rep., NASA Lewis Research Center, Cleveland, OH (United States), 1982.

[11] Sodja, J., Drazumeric, R., Kosel, T., and Marzocca, P., "Design of Flexible Propellers With Optimized Load-Distribution Characteristics," *Journal of Aircraft*, Vol. 51, No. 1, 2014, pp. 117–128.

[12] Bocci, A., "A New Series of Aerofoil Sections Suitable for Aircraft Propellers," *Aeronautical Quarterly*, Vol. 28, No. 1, 1977, pp. 59–73.

[13] Martins, J. R., and Ning, A., *Engineering Design Optimization*, Cambridge University Press, 2021.

[14] Lv, P., and Gangoli Rao, A., "Conceptual Analysis of Boundary Layer Ingestion Towards Aircraft Propulsion Integration," *Proceedings of the XXI International Symposium of Air Breathing Engines*, American Institute of Aeronautics and Astronautics Inc. (AIAA), 2013, pp. 1–15.

[15] Hartman, E. P., and Biermann, D., "The Aerodynamic Characteristics of Full-Scale Propellers Having 2, 3, and 4 Blades of Clark Y and R.A.F. 6 Airfoil Sections," Tech. Rep. NACA-TR-640, National Advisory Committee for Aeronautics (NACA), 1938.

[16] Goyal, J., "Blade Element Momentum Theory Code for Positive and Negative Thrust Propellers," , 2024. https://doi.org/10.4121/E748A68D-5F15-4757-B904-880BCEC8217B.V1.